COUPLING BETWEEN FLUID DYNAMICS AND

ENERGY ADDITION IN ARCJET AND

MICROWAVE THRUSTERS

Final Technical Report

Dr. Michael M. Micci
Department of Aerospace Engineering
The Pennsylvania State University
University Park, PA   16802

For the period:

1/2/85 - 1/1/86

Submitted to:

ABSTRACT

A new approach to numerically solving the problem of the constricted electric arcjet is presented. An Euler Implicit finite difference scheme is used to solve the full **compressible Navier Stokes equations in two dimensions.** The boundary and initial conditions represent the constrictor section of the arcjet and hydrogen is used as a propellant. The arc is modeled as a gaussian distribution across the centerline of the constrictor.

Temperature, pressure and velocity profiles for steady state converged solutions show both axial and radial changes in distributions resulting from their interaction with the arc energy source for specific input conditions. The temperature rise is largest at the centerline where there is the greatest concentration of arc energy. The solution does not converge for all initial inputs and the limitations in the range of obtainable solutions are discussed.

N86-22891 #

TABLE OF CONTENTS

LIST OF FIGURES

Chapter I

INTRODUCTION

1.1 Review of Arcjet Propulsion

The concept of electric propulsion has been intro-
duced as an alternative to the chemical liquid and solid
rocket. The idea was an outgrowth of the increasingly
popular arc heaters being used in the late fifties and
early sixties in wind tunnels for reentry simulation. One
of the most significant advantages to using electric pro-
pulsion is the tremendous increase in specific impulse
(thrust per unit mass flow) over conventional rockets. On
the average, the electric thruster can get ten times more
specific impulse than the solid rocket engine. The main
focus of arcjet research is for orbit-maneuvering applica-
tions. The high specific impulse means less fuel has to be
boosted into orbit and that high payload capabilities are
promising. The arcjet can generate low levels of thrust
for long periods of time, but in general the transfer times
for these systems tend to be longer than for other propul-
sive systems.[1]

Various configurations of electric arc heaters
exist, but the one more frequently used for propulsive

purposes is the concept of the constricted arc (see Fig. 1). The arc itself is an electric discharge capable of sustaining large currents between two electrodes, from the negative cathode to the positive anode. The arc is contained in a narrow constricted duct which keeps it from dissipating before it reaches the diverging nozzle. The purpose of the constrictor is to provide stability and restrict the movement of the arc to prevent radial kinking.[2] Gas enters axially into the constrictor from either side of the cathode, absorbing energy from the arc and accelerating as it flows through the section. The moving gas keeps the arc from attaching to the walls. Negligible heat conduction takes place between the edges of the arc and the walls, therefore the cool layer of gas lets the wall temperatures remain fixed. The gas expands in the divergent nozzle at the constrictor exit thereby producing thrust. The arc attaches to the anode at the downstream end of the constrictor.

Previous work with propellants reveals that the lower the molecular weight, the higher the exhaust velocity that can be obtained.[1] A propellant with low molecular weight produces higher levels of specific impulse, such as those being used in the current analysis. At these levels, the maximum arc chamber temperature using hydrogen will be lower than for any other known propellant to obtain the
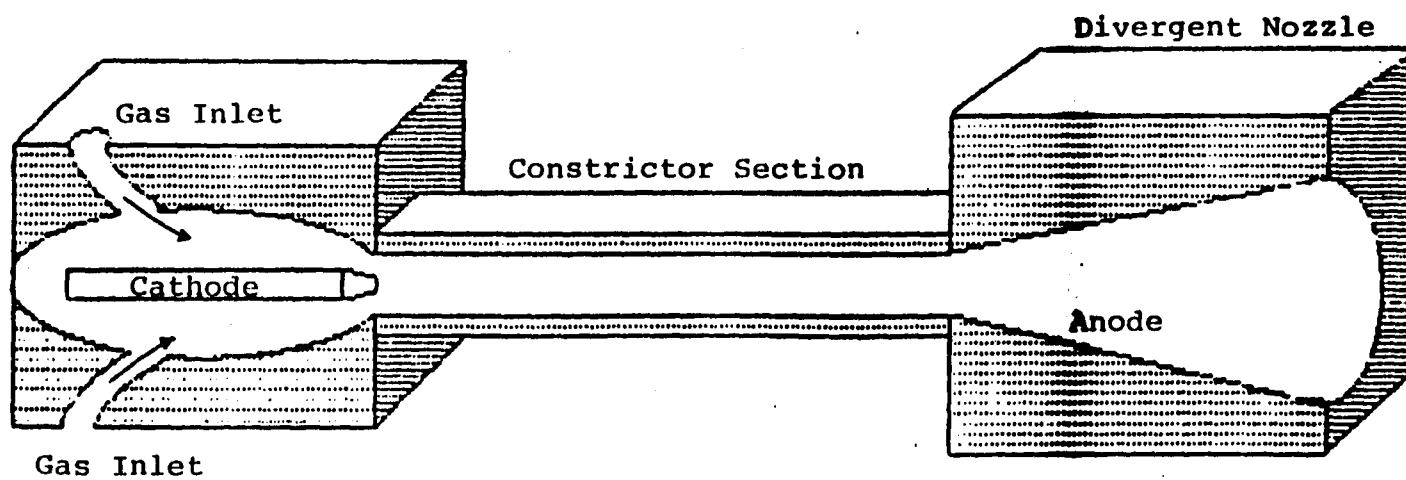
Figure 1. The Constricted Arcjet Engine

same specific impulse.[3] Although still not altogether
practical because of storage problems, hydrogen is consid-
ered an efficient and desirable propellant for applications
of this kind. In addition, accurate data of hydrogen gas
properties are readily available and are not considered to
be a significant source of error in numerical calculations.

1.2 Previous Theoretical Work

In the early sixties there was a considerable effort
made to solve, both experimentally and theoretically, the
problem of the wall-constricted, direct current electric
arc. Several analytical models were developed before
numerical solutions were available. Although the linear-
ization of the equations and the necessary assumptions that
must be made for the analytical solution limit their
effectiveness, significant overall trends can be determined
and are helpful as a first approximation.

The simplest analytical solution to the constricted
arc problem is the Stine-Watson model.[4] In 1962, H. Stine
and V. Watson modeled an arc air-heater, linearizing and
uncoupling the energy equation so that it could be solved
using modified Bessel Functions in one dimension. The
simplified second order energy equation is defined in terms
of the conductivity function, $S = \int \sigma(T)dT$, which is intro-
duced so that the energy equation becomes

$$\rho V_z \frac{\partial h}{\partial z} = \sigma E^2 + \frac{\partial^2 S}{\partial r^2} + \frac{1}{r} \frac{\partial S}{\partial r} + \frac{\partial^2 S}{\partial z^2} \qquad (1)$$

where σ is the local electrical conductivity, E is the voltage gradient, h is the local enthalpy, V_z is axial velocity, ρV_z is assumed to be a constant, the flowfield is laminar and steady, and the air is treated as being in thermodynamic equilibrium.[5]

As shown in Figure 2a, the stationary arc is assumed to take up a large fraction of the constrictor diameter. The mass flux is assumed constant, axial pressure gradients are assumed negligible and only heat loss due to thermal conduction is considered. The analysis takes place only within the arc column region, which does not take into account flow passing the cathode and anode. The results show the axial and radial effects of enthalpy inside the column as well as voltage gradients and electrical conductivity. Further experimentation has shown that despite the shortcomings in the analytical approach, this analysis predicts fairly well the energy distribution inside the column.

The first significant analytic thruster model is known as the Core-Flow model. The basic difference between the Core-Flow theory and the Stine-Watson model is the assumption of a thin arc with respect to the constrictor

diameter and the exclusion of axially dependent terms from the energy equation. The enthalpy of the core is assumed to be given by the Elenbaas-Heller equation and is independent of the mass flow.[5] The basic energy equation, after the axial conduction and convection terms are neglected, reduces to

$$\sigma E^2 = P_r - \frac{1}{r}\frac{\partial}{\partial r}(r\frac{dS}{dr}) \tag{2}$$

where P_r is the local radiated power per unit volume.

As illustrated in Figure 2b, the gas flow in the constrictor is broken down into several regions; the hot central core where gas is heated directly by the arc, the inner flow in which the gas is heated by conduction and an outer flow which is heated by contact with the constrictor walls. Most of the mass flow occurs in the cool outer flow region with negligible flux assumed through the core.

The poor representation of axial enthalpy flux as well as energy flux inside the column at the constrictor entrance and exit limit the applicability of the solutions. However, the model does give a realistic picture of the mass flux at the constrictor inlet and of the overall enthalpy distribution.[6] The core flow model predicts strong gradients in temperature, density and velocity at the inlet, and results indicate that the maximum amount of thrust is obtained by a steady and uniform flow.[7] The
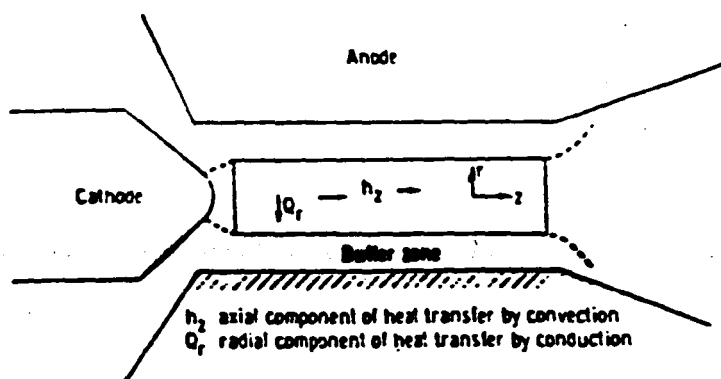
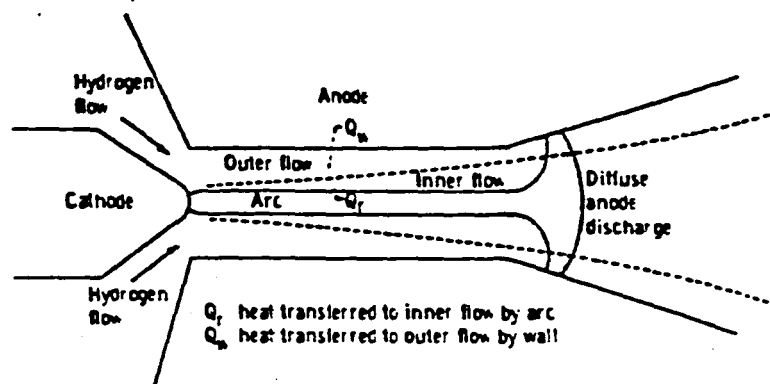**Figure 2a.** Mechanisms of Heat Transfer in Stine-Watson Theory [5]

Figure 2b. Regions of Flow and Energy Source for Each in Core-Flow Model [5]

performance estimates produced by the Core-Flow model are
useful approximations and the analysis shows that the
performance of the arcjet is directly related to the amount
of flow losses.

The most extensive numerical solution at that time
was done by Watson and Pegot[8] as a comparison to the Stine-
Watson model. The basic theoretical models were the same
except fewer simplifying assumptions were made in the
numerical solution. The analysis of the coaxial flow was
carried out using a finite difference scheme for varying
sizes, enthalpy levels and pressure levels. The idea was
to study the behavior of the wall-constricted arc in the
range where radiation heat loss is a noticeable portion of
the total heat loss from the system. Results showed little
difference between the solutions and that the qualitative
trends were the same. Watson concluded that the major
effect of large radiation losses was to lower and flatten
the enthalpy distribution.

Another numerical solution of the flow conditions
inside an arcjet was presented in 1962 by P. Masser[9], using
a completely different approach than that of Watson and
Pegot, and involving the solutions to the equations of
momentum, energy, continuity, and Ohm's law. The analysis
assumes the flow is one dimensional, with axial symmetry
and that pressure is only a function of x. Axial heat flow

is neglected and all the upstream properties are assumed
given initially. The results show velocity, enthalpy and
voltage gradients at various axial locations for hydrogen
gas and a particular set of input. Recently, Masser used
an updated version of his program[10] to compare the results
with previous related works, in particular, with Watson's
numerical results[8] and the experimental results of Todd and
Sheets[3]. He then studied the effects of varying certain
parameters, such as velocity and enthalpy. He again makes
simplifying assumptions to solve the necessary set of
equations: continuity, momentum, energy and Ohm's law.
Masser concludes that his solutions are in reasonable
agreement with Todd and Sheets and shows that his voltage
and enthalpy gradient profiles closely match those of
Watson. Results also indicate an increase in performance
of the engine and better correlation with other results as
the arc chamber length is increased.

1.3 Current Analysis

A new approach to solving the two dimensional
Navier-Stokes equations numerically has been developed
recently by C. Merkle, G. Molvik, and D. Choi[11]. The
original application was to solve a compressible or incom-
pressible laser heat addition problem. For the case of
the arcjet, the geometry was adapted to represent the

constrictor section of the arcjet and the heat addition modified to represent a concentrated source on the center-line of the constrictor. Analytical and numerical work on this problem to date has not completely included the effects of viscosity in the equations. The code can be modified to model several different boundary conditions that depend on which specific initial conditions are being used.

The solution consists of formulating the equations into matrix form and applying an Euler-Implicit finite difference scheme. The gas flow inside the constrictor is taken as laminar and only steady state solutions are con-sidered. A power source term is added to the energy equa-tion for the arc, viscosity is taken into account, and real gas properties are used in solving for the local thermo-dynamic properties inside the constrictor. The energy input is assumed constant in the axial direction, falling off radially in a gaussian distribution to zero at some specified distance from the centerline. The heat is assumed to start at the tip of the cathode and stop at the constrictor exit. The region covered in the analysis and the representative finite difference grid spacings are shown in Figure 3. The steep gradient of cool to hot gas in the constrictor produces a highly two dimensional flow-field.[12]
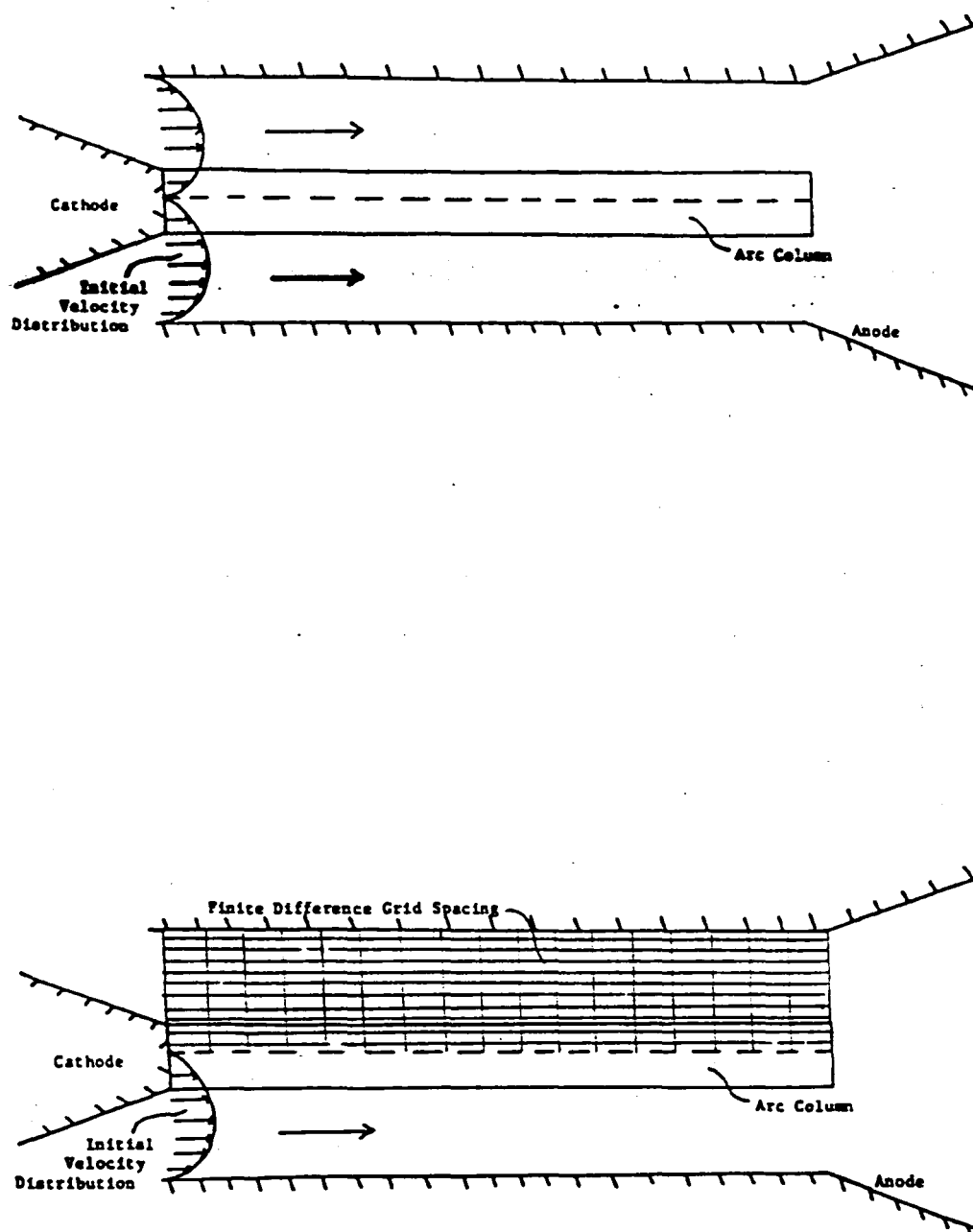

Figure 3.   Constrictor and Nozzle Geometry

Chapter 2

FORMULATION OF THE PROBLEM

2.1 Governing Equations

The two-dimensional unsteady compressible Navier-Stokes equations are used[12] to describe the flow in the constrictor. In cartesian coordinates the conservation vector form of these equations is

$$\frac{\partial Q}{\partial t} + \frac{\partial E}{\partial x} + \frac{\partial F}{\partial y} = \frac{\partial V}{\partial x} + \frac{\partial W}{\partial y} + H \tag{3}$$

where

$$Q = \begin{pmatrix} \rho \\ \rho u \\ \rho v \\ e \end{pmatrix} \quad E = \begin{pmatrix} \rho u \\ \rho u^2 + p \\ \rho u v \\ (e + p)u \end{pmatrix} \quad F = \begin{pmatrix} \rho u \\ \rho u v \\ \rho v^2 + p \\ (e + p)v \end{pmatrix} \quad H = \begin{pmatrix} o \\ o \\ o \\ q(x,y) \end{pmatrix} \tag{4}$$

In addition, ρ = density, u = axial velocity, v = radial velocity, p = pressure, e = internal energy, and q = heat.

In this analysis, ρ, ρu, ρv, and e are the dependent variables, which are contained in the vector Q. The equations are solved in terms of these parameters, namely continuity, x-momentum, y-momentum, and energy. The flux vectors E and F represent the convective terms, V and W are

12

the viscous terms and H is the source term. The viscous terms incorporate all shear stresses and there is a pressure dependence in both the x and y directions implying full consideration of the pressure gradients[12]. An expanded component form of the above governing equations is contained in the appendix.

Pressure is obtained from the equation of state

$$P = \frac{\rho R T}{M_w} \qquad (4)$$

where ρ = density, R = universal gas constant, T = absolute temperature and M_w = molecular weight.

The source term added to the energy equation is a guassian distribution, $(P = e^{(-bx^2)})$, that is specified as taking up a certain percentage of the constrictor diameter. The percentage of the total diameter that is covered by the arc is defined as Percent. The quantity Py is subsequently defined from this as

$$Py = (1 = Percent)Y_{max} \qquad (5)$$

where Y_{max} is the constrictor radius. Ther term b is defined as

$$b = \frac{\log(\frac{1}{P_{max}})}{(Py - Y_{max})^2} \qquad (6)$$

and finally, the power P becomes

$$P = P_{max} \, e^{b(Y_{max} - y)^2} \tag{7}$$

where P_{max} is the specified maximum power input along the centerline, y being the radial coordinate above the wall of the constrictor. This is empirically shown in Figure 4. The power is added directly to the energy equation in SI units of W/m^3, where the third dimension is considered to be of unit length and the energy input remains constant through each iteration.

The equations are written in a generalized coordinate system in order to simplify the curvilinear grid generation. Although this is not necessary for the particular case studied here, any future adaptations to the shape of the constrictor can be obtained with only minor modifications to the geometry specifications in the code.

2.2 Euler-Implicit Method of Solution

The governing equations are solved using a time dependent finite difference scheme. The term Euler-Implicit means that the first order differences with respect to time are implicit and the solutions are unconditionally stable. The partial derivatives with respect to space are then second order differences. Viscosity and the power source are handled explicitly throughout in the terms on the
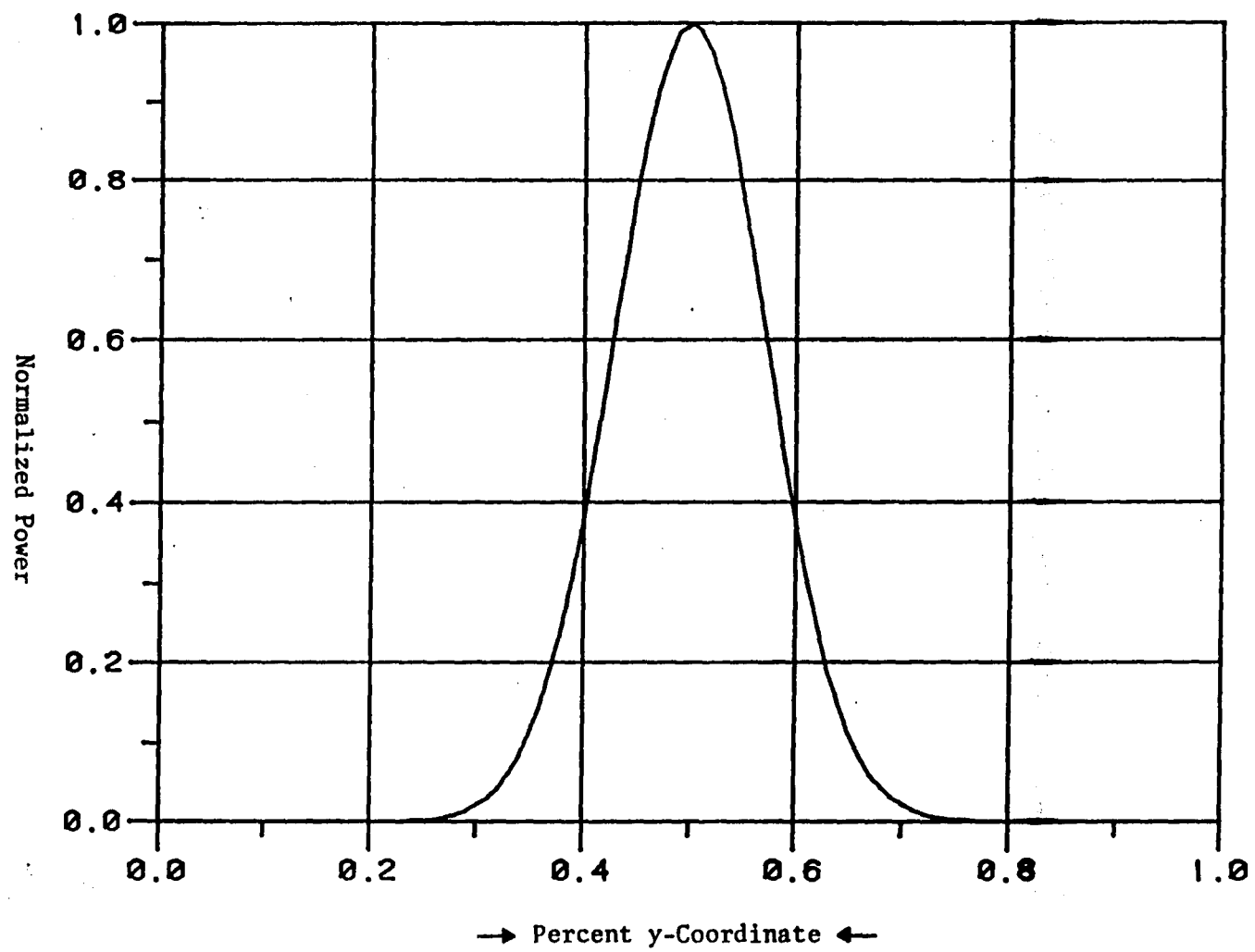
Figure 4. Power Distribution of Arc vs. Radial Coordinate

right hand side of the equations. All terms on the left hand side of the equations are solved implicitly. The equations are solved in conservation form so that mass, momentum and energy are conserved identically and linearization is required only with respect to time.[13]

As stated previously, the vector form of the Navier-Stokes equations is

$$\frac{\partial Q}{\partial t} + \frac{\partial E}{\partial x} + \frac{\partial F}{\partial y} = \frac{\partial V}{\partial x} + \frac{\partial W}{\partial y} + H \tag{8}$$

Solving these equations simultaneously using the Euler-Implicit scheme requires writing them in delta notation. To do this, we first define the Jacobian matrixes A and B as

$$A = \frac{\partial E}{\partial Q} \quad \text{and} \quad B = \frac{\partial F}{\partial Q} \tag{9}$$

The original delta form of the equation is

$$(I + \Delta t \frac{\partial A}{\partial x} + \Delta t \frac{B}{\partial y}) \Delta Q = -\Delta t [\frac{\partial}{\partial x}(E-V) + \frac{\partial}{\partial y}(F-W) - H] \tag{10}$$

Since the terms on the right hand side of the equation are solved explicitly, they can be referred to simply as the quanity

$$RHS = -\Delta t[\frac{\partial}{\partial x}(E-V) + \frac{\partial}{\partial y}(F-W) - H] \tag{11}$$

The Douglas-Gunn approximate factorization[14] is applied to the equations at each time step. The implicit terms are written in the form

$$(I + \Delta t\frac{\partial A}{\partial x})(I + \Delta t\frac{\partial B}{\partial y})\Delta Q = RHS \tag{12}$$

$\Delta Q*$ is now defined as

$$\Delta Q* = (I + \Delta t\frac{\partial B}{\partial y})\Delta Q \tag{13}$$

and then

$$\Delta Q* = (I + \Delta t\frac{\partial A}{\partial x})^{-1}RHS \tag{14}$$

so the above equation can be rewritten

$$(I + \Delta t\frac{\partial A}{\partial x})\Delta Q^* = RHS \tag{15}$$

The desired quantity ΔQ can now be written as

$$\Delta Q = (I + \frac{\partial A}{\partial x})^{-1}\Delta Q* \tag{16}$$

Blottner's block solver[15] is used to solve the block tridiagonal matrix first for the vector $\Delta Q*$ and then once again for ΔQ.

The quantity ΔQ is used as the basis for computing the values at the next time step. The quantities making up ΔQ are $\Delta\rho$, $\Delta\rho u$, $\Delta\rho v$, and Δe. These quantities are added to the previous value at that location and all thermodynamic properties are computed from these relationships.

A constant time step is used in the iterations for simplicity. A variable time step produces a faster convergence, but is not necessary for the steady state solution used. The time step size is a function of the CFL condition for stability and is limited by the value of the CFL. If the CFL is too large or too small, the solution will not converge. The time step is obtained from the inputed CFL and the maximum eigenvalue from the Jacobian matrices A and B, which is a function of the speed of sound. The CFL value used is 5, which is considered optimum by experimentation.

2.3 Boundary and Initial Conditions

The most important criteria for correctly solving the Navier-Stokes equations using the Euler-Implicit scheme is to have valid boundary conditions. The finite difference grid for the constrictor diameter is generated first in rectangular coordinates from the specified number of x and y points needed for an accurate analysis, and then transformed to generalized coordinates $\xi(I,J)$, $\eta(I,J)$. The J=1 location corresponds to the lower constrictor wall, J=JL

represents the upper wall, I=1 is the inlet and I=IL is then the constrictor exit, as Figure 5 shows.

The initial upstream conditions specified are stagnation pressure, stagnation temperature, and a variable velocity distribution. Downstream, a constant pressure is imposed at the constrictor exit. The code was determined to work best for cases with a constant velocity profile and slip conditions at the wall, which corresponds to higher Mach number, compressible flow conditions. The constant velocity profile is defined as u=constant along the entire inlet location. No radial component in the initial velocity is assumed, which is written in the form arctan v/u = 0.
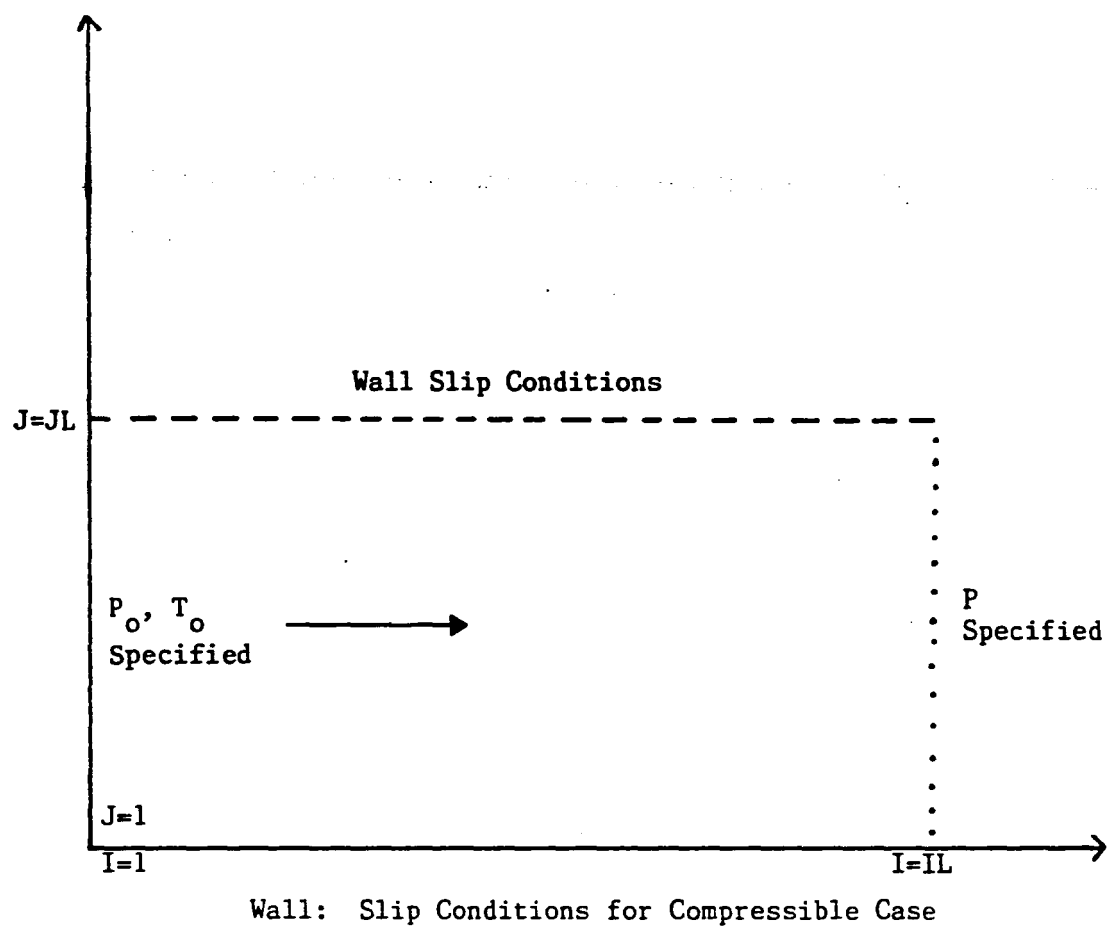
Wall: Slip Conditions for Compressible Case

Figure 5. Boundary Conditions on the Constrictor

Chapter III

NUMERICAL RESULTS AND DISCUSSION

3.1 Cold Flow Results

Convergence is most important in an iterative
solution over time. The solution is not completely correct
until the dependent variables no longer change with respect
to time. These parameters, $\Delta\rho/\rho$, $\Delta\rho u/\rho u$, $\Delta\rho v/\rho v$, $\Delta e/e$,
become zero when the solution has reached complete conver-
gence. The system is then considered to continue in steady
state. A solution diverges when one or more of the input
data are incompatible with the set boundary conditions of
the problem. The input conditions in this analysis that
can be varied to simulate a certain system are the inlet
stagnation temperature (T_0), the inlet stagnation pressure
(P_0), the back pressure, the amount of energy input per
cubic meter of the arc (Power), and the physical size
of the constrictor section. In addition, significant
differences in the solution occur with changes in the
grid size. The number of iterations required to reach
a converged solution changes with the grid size and to
a lesser extent with the specific initial conditions.

21

Simple test cases of the program were run to determine if a converged solution was obtainable with the modified heat input and initial conditions. A solution is easily predicted for a uniform flow with no heat addition; with a constant velocity profile, slip conditions at the walls, and uniform initial temperature and pressure radially, the flow should remain unchanged because it is already in steady state. After several different sets of initial conditions were run, the flow characteristics remained constant with time and all convergence parameters began and remained at zero. These results were consistent throughout any variation in geometry or grid spacing.

The final range of initial conditions used in this study are similar to those successfully used in other applications of this code and are representative of real situations that might occur inside a constricted arc. Stagnation temperatures range from 800° to 3200°K, inlet Mach numbers run between .18 and .5, and stagnation pressures are between 1 and 6 atms. The physical size of the constrictor sections modeled ranged between lengths of .1 and .25 m and heights between .025 and .1 m, however, throughout the study it was noticed that the actual physical size of the constrictor channel did not affect convergence. The number of grid points chosen in the x-direction is in every case much smaller than the number of points

chosen in the y-direction because the property profiles change much more drastically across the diameter than from one axial location to another. Faster convergence occurs with a coarser grid mesh, however in most cases a finer grid mesh was used because of the increase in accuracy of the solutions.

The parameter with the greatest effect on the convergence of the solution is the power input. The actual percentage of area covered by the arc and its corresponding percentage of the maximum possible power in that area determine how many Watts of power are emitted into the constrictor. The power inputs run between 1.2×10^2 W and 1.8×10^5 W, or 1×10^9 and 1.5×10^{12} W/cm^2, where the value stated represents the level of power at the centerline which falls off in a gaussian distribution to zero at a distance of 20 percent in the constrictor diameter on either side of the centerline.

3.2 Effect on Power Input

Once it was successfully determined that the code was valid for a uniform flow with no heat source, energy could be added in small increments to determine the effect of the presence of the arc on the flow characteristics of the moving gas and convergence of the solution. The solutions to the code are outputted in the form of the values

of the local thermodynamic properties at each point on the grid after the desired number of iterations. The most important of these parameters is temperature, which is a direct indication of how much energy is being absorbed by the hydrogen gas from the arc.

The lowest power input to record a significant temperature rise was 1×10^9 W/cm^2 where the initial conditions used were a stagnation temperature T=1500°K, a stagnation pressure of P=3 atm, and an inlet Mach number of M=.254, using a grid size of 11 by 20. The actual size of the constrictor was .15 m long by .05 m high. The solution quickly converges to zero and the maximum temperature rise was 2°K, which occurs on the centerline at the exit. Convergence was also computed for power levels of 1×10^{10}, 1×10^{11} and 1×10^{12} W/cm^2. Figure 6 shows a log-log plot of power input vs. ΔT and indicates that as the power increases by a factor of ten, the maximum temperature rise also increases by a factor of ten. Convergence plots for these cases indicate that the lower the power input, the faster the convergence. This implies that the lower the heat addition, the less disruption is introduced into the systems and the faster the system can reach a steady state.

The converged solutions were checked by determining if energy was conserved in the system. The energy at the inlet, added to the energy of the heat addition inside the
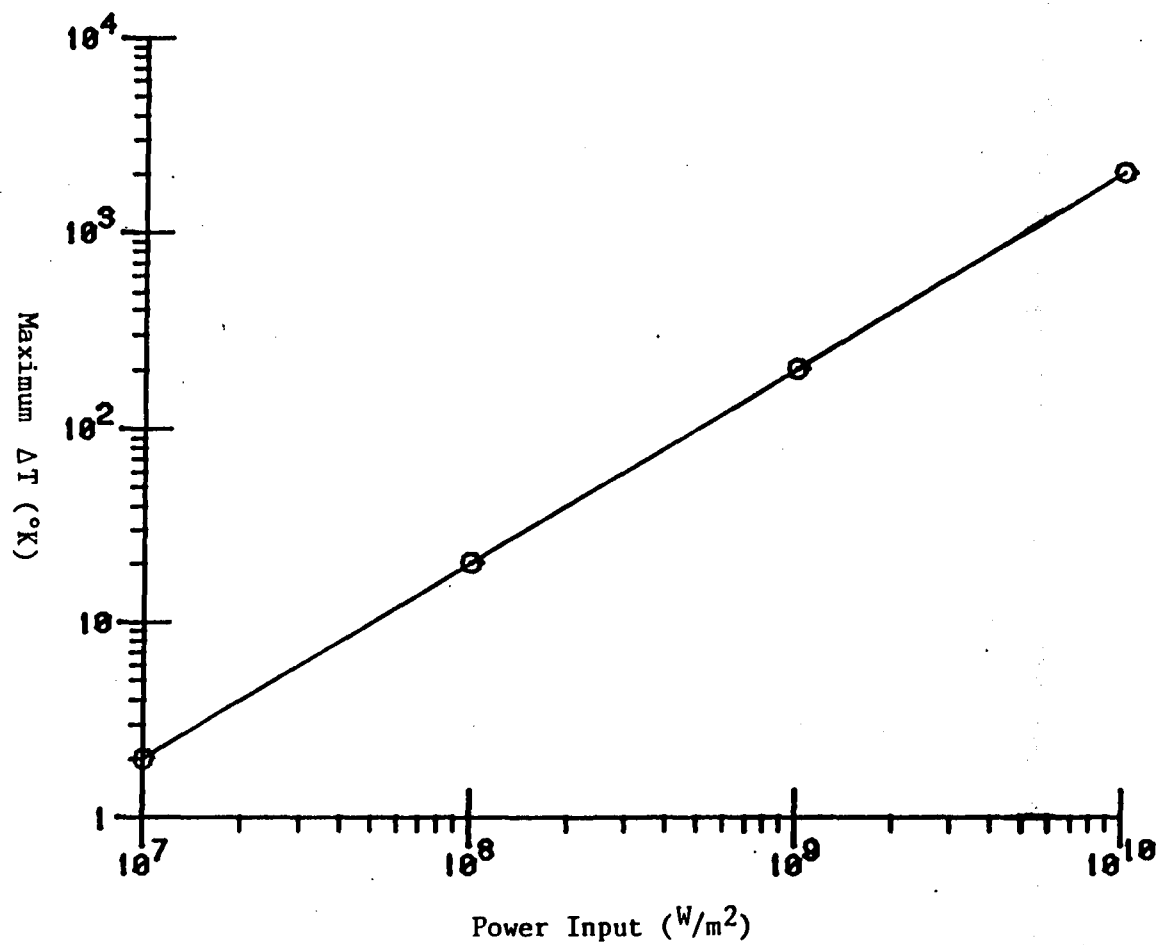
Figure 6.   Log–Log Plot of Power Input vs. Maximum Change
in Temperature of Constrictor

constrictor should equal the energy at the exit. The program has internal limitations as to the accuracy of the corner grid points at the inlet and exit and the calculations were performed with increased accuracy at axial locations one point after the inlet and one point before the exit, I-2 and I=IL-1.

The energy difference between the inlet and the exit is calculated by solving the following equation,

$$Q = \int_{out} (e + p)udy - \int_{in} (e + p)udy \qquad (17)$$

where Q is the power of the arc in Watts. A program was designed to take the converged solution variables, e, p, and u and automatically integrate the inlet and exit energies. The quantity Q is determined by the amount of area in the entire constrictor that is actually covered by the arc. These calculations show consistent error of 6 to 7 percent between the difference in power from the inlet to exit and the power inputed from the arc. This is considered reasonable because errors may be introduced in the exact calculation of Q.

Although there is no lower bound heat input for this code, there is an upper limit to the amount of energy that can be introduced into the system and still reach a converged solution. For a given set of initial conditions,

when the power per square meter is raised past a certain value, the dependent parameters, $\Delta Q/Q$, become so large that they caused an arithmetic fault in the program. The limit was found to be somewhat dependent on the fineness of the grid spacings but overall the power level could not be raised higher than about 1×10^{12} W/cm^2 corresponding to a ΔT of about 2000°K.

Figure 7 shows the temperature cross section at the axial location just before the exit, where the grid points were 11 x 40. For given conditions of initial stagnation temperature T=2000°K, stagnation pressure P=4 atm, constant inlet Mach number M=.19 and Power=1×10^{12} W/cm^2, the maximum ΔT is 1800 degrees. The cross section is similar to the gaussian power input profile (Figure 4) except appears wider. As expected, the temperature is highest where the concentration of energy is greatest. Figure 8 shows the log-linear plot of the convergence criteria for this case. $\Delta \rho/\rho$, $\Delta \rho u/\rho u$, $\Delta \rho v/\rho v$ and $\Delta e/e$ become zero as the steady solution approaches. The $\Delta Q/Q$ terms do not smoothly approach zero, but rather take short jumps up and down while gradually decreasing toward zero. In every case run, the x-momentum took the most iterations to converge to zero. The program was run again, increasing the power input to 1.3×10^{12} W/cm^2 and after 165 iterations, the $\Delta Q/Q$ diverged and the code automatically stopped. The code can allow only
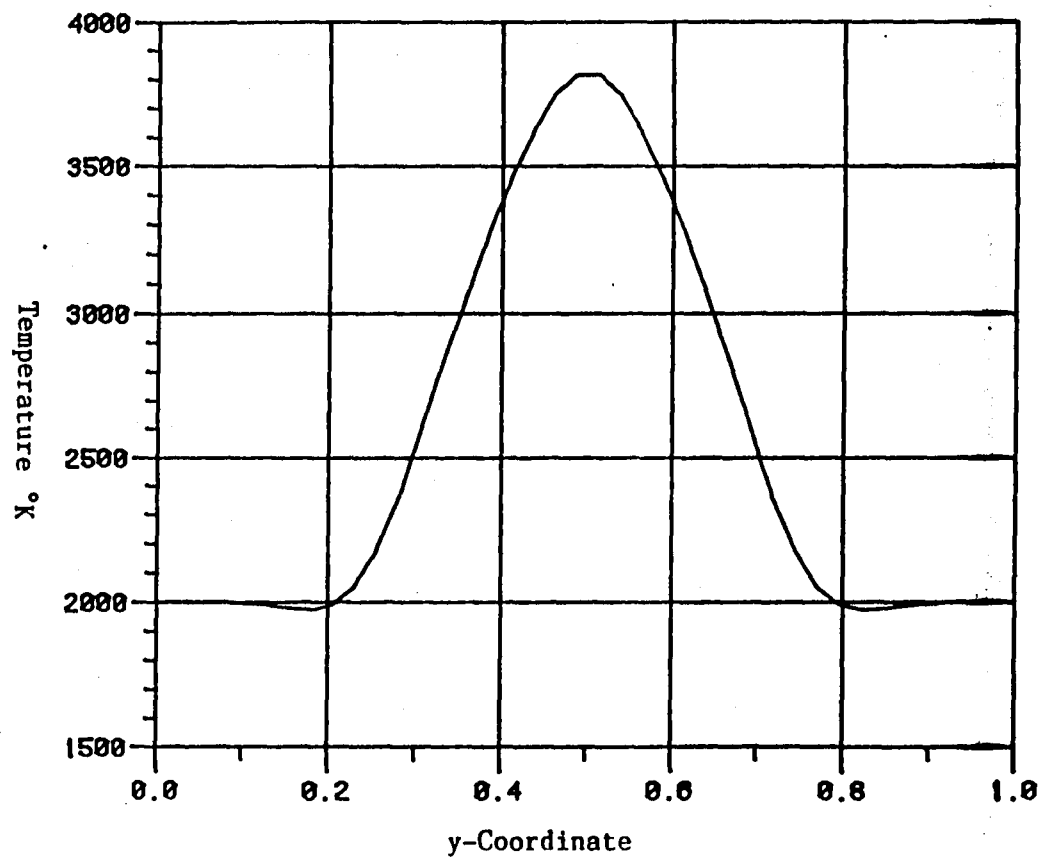
Figure 7. Temperature Profile Across the Constrictor for Test Case (T=2000°K, P=4 atm, M=.19, Power= 1×10^{12} W/cm^2)
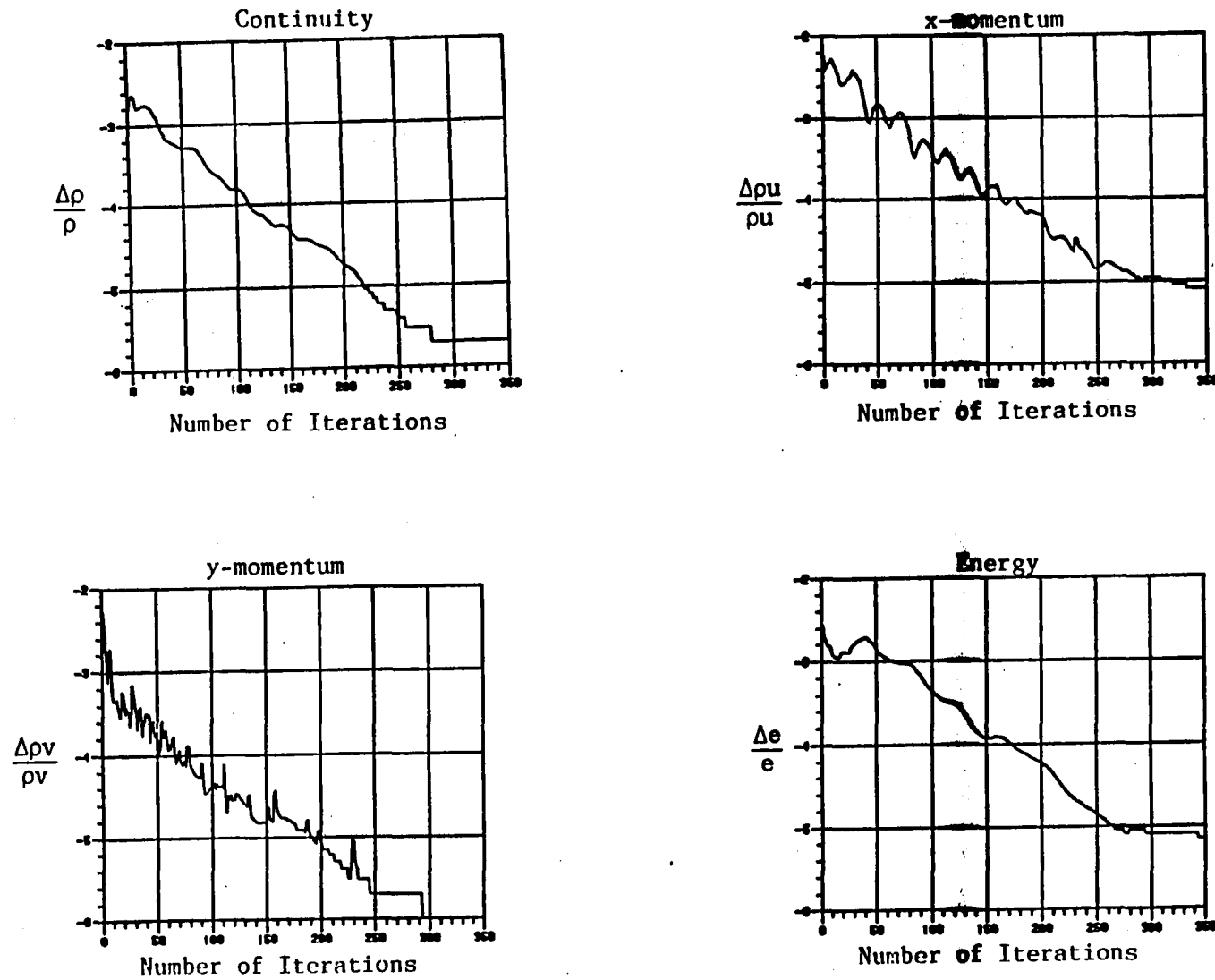
Figure 8.   Convergence of Dependent Variables for Test Case
(T=2000°K, P=4atm, M=.19, Power=1.3x10^{12} W/cm^2)

so much energy input into the constrictor before the energy
equation registers a discontinuity which affects the energy
convergence and ultimately the rest of the convergence
parameters. However, it is interesting to note that the
solution begins with ΔQ/Q decreasing normally, then suddenly
within only a few iterations the corrections increase
dramatically and the solution fails. Figure 9 shows the
drastic change in ΔQ/Q. The values jump to hundreds of
times their initial values before the code stops because of
an arithmetic fault.

3.3 Effect of Temperature Initial Conditions

Initial inlet and wall temperatures have an effect
on the maximum overall change in temperature of the con-
strictor for a given value of energy input. Six cases were
run with all the same conditions except the initial temper-
ature was varied. Figure 10 shows the temperature profiles
at the exit axial location. The initial conditions used
are P=4 atm, and T=400°, 800°, 1400°, 2000°, 2600°, and
3200°K. Note that as the inlet temperature increases, the
maximum change in temperature on the centerline decreases,
but in each case the profiles have the same shape. When
T=800°K, the ΔT was 2300 degrees whereas with 3200°K, the
maximum temperature change was only approximately 800°K.
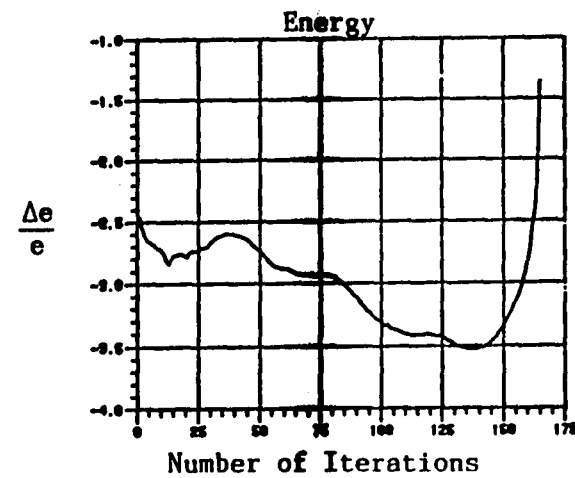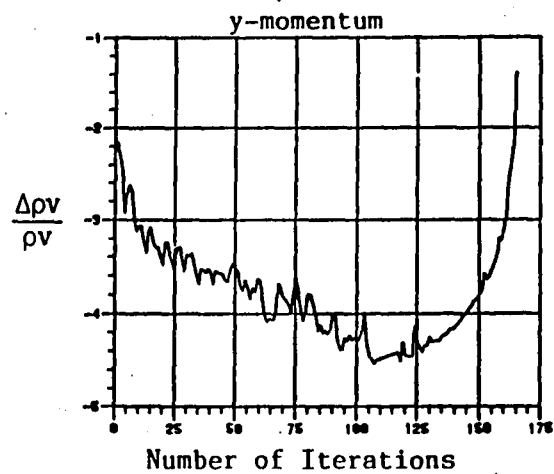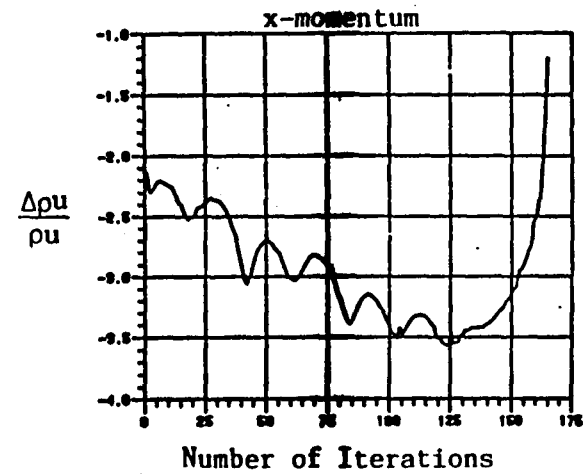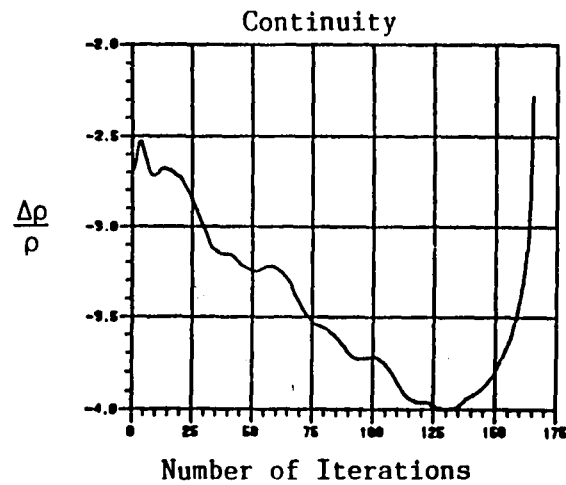The solution diverged, however, when run with temperatures

Figure 9. Divergence of Dependent Variables For Test Case
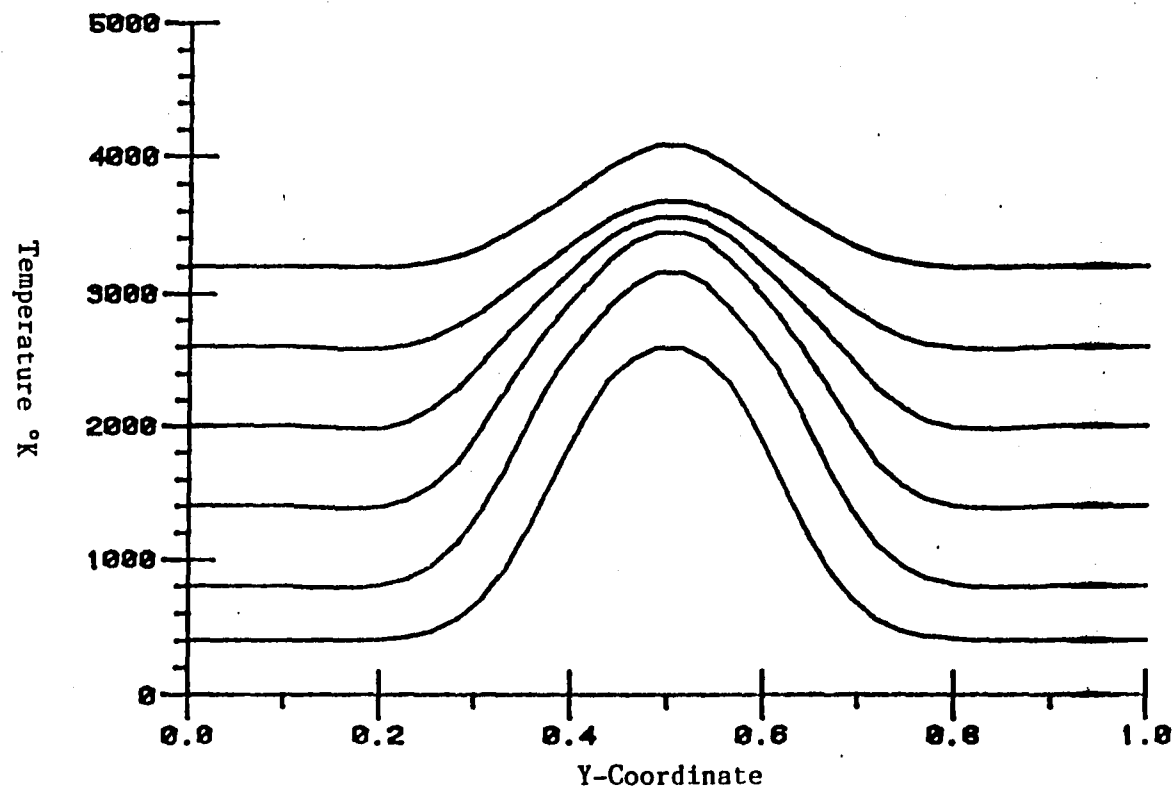(T=2000°K, P=4 atm, M=.19, Power=1.3X10^{12} W/cm^2)

Figure 10. Temperature Cross Section at Exit for Various
Initial Temperatures (P=4 atm, Velocity=750 m/sec,
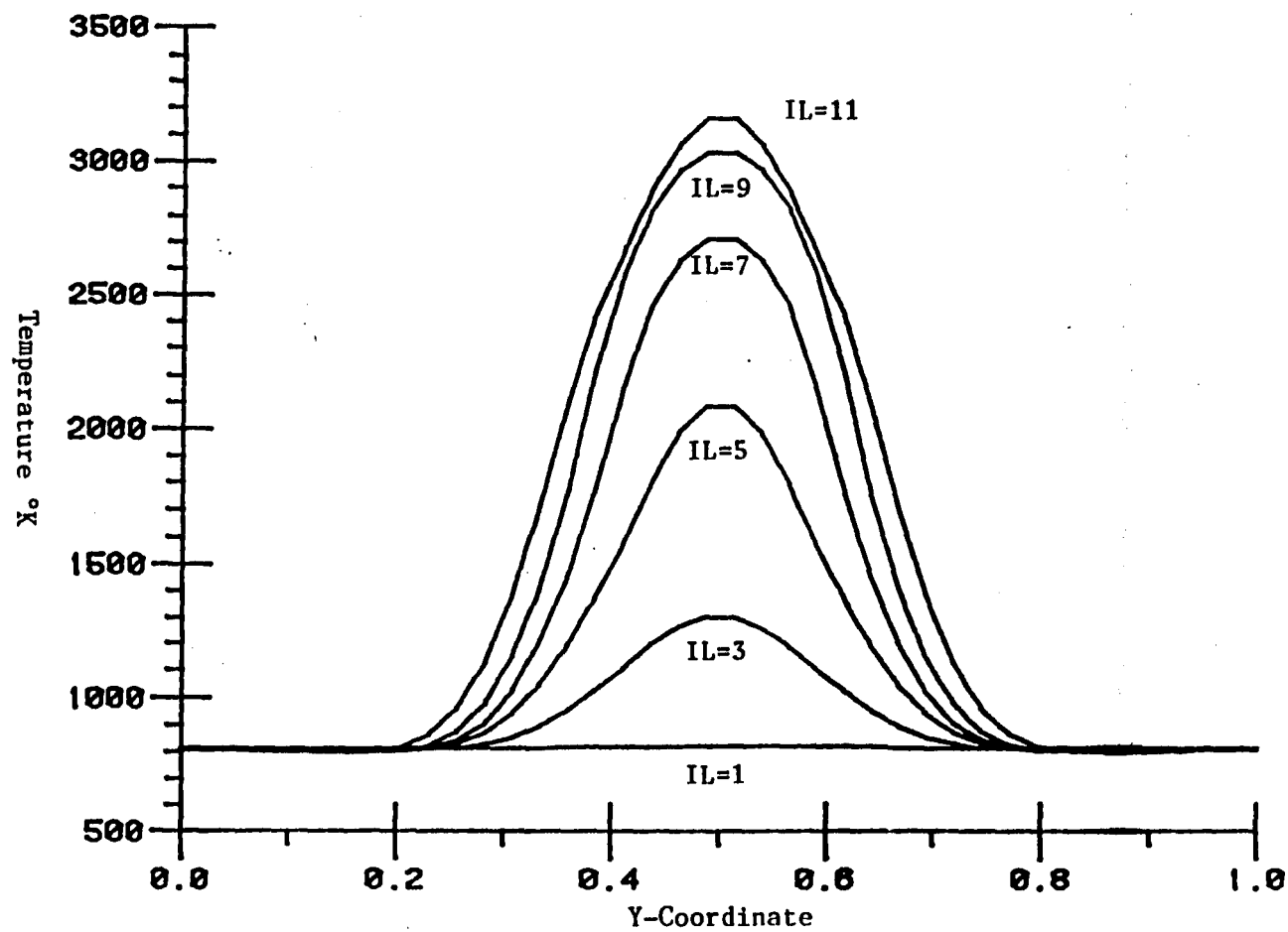Power=1.5 x 10^{12}W/cm^2)

Figure 11. Temperature Cross Sections at Various Axial Locations
(T=2000°K, P=4 atm, M=.35, Power=1.5X10^{12} W/cm^2)

below 400°K, implying that there is at least a lower limit
for temperature in the range of obtainable solutions.

Figure 11 shows the axial change in temperature
profiles for the case of T=800°, P=4 atm, and M=.348, with a
power input of 1.5×10^{12} W/cm^2. The local temperature cross
section is plotted for x locations of IL=1,3,5,7,9 and 11,
where IL=1 corresponds to the inlet and IL=11 is the exit.
The maximum temperature for this completely converged
solution occurs at the exit, as well as the maximum
velocity.

3.4 Effect of Velocity and Pressure

Both velocity and pressure changes affect the conver-
gence and temperature rise in the constrictor. The velocity
distribution does not remain constant after the heat source
is introduced into the system. Figure 12 shows the velocity
distributions for the same initial conditions and axial
locations as the above temperature profiles in Figure 11.
The velocity starts out as a constant across the inlet but
as the program is run and heat is added, the velocity
decreases in the center region due to interaction with the
arc. The velocity increases fairly steadily as it moves
downstream until right before the exit where it takes an
unprecedented jump at the center while forming wells of low
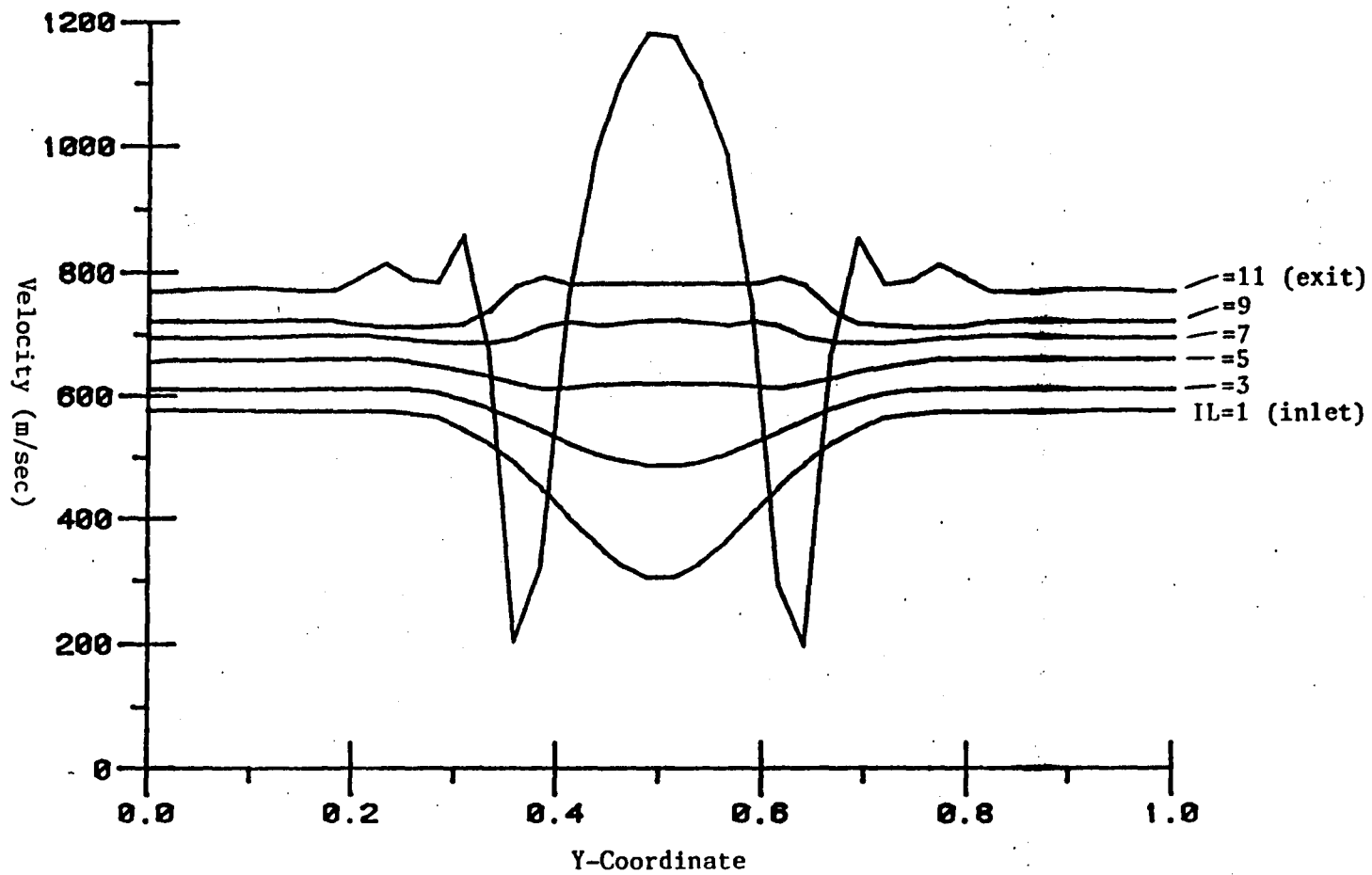velocity points on either side of the centerline. At the

Figure 12.   Cross Sectional Velocity Profiles at
Various Axial Locations

same time, with heat inputs above $1x10^{11}$ W/cm^2, the velocity gradients in the y-direction become significant, causing the flow to become very turbulent in the center region. However, the velocity remains radially uniform throughout the channel outside the region of the arc.

Pressure follows a similar but opposite pattern to the velocity distribution as can be seen in Figure 13. The pressure begins by rising at the inlet in the center of the constrictor but decreases consistently and forms a more linear profile as it moves axially downstream, decreasing over 10 percent from its initial value of 4 atm when it reaches the exit.

A lower limit is also apparent for possible initial stagnation pressures for a specific set of input. For example, one case was run with an initial temperature T=1500°K, an inlet Mach number M=.254, and a power input Power=$5x10^{11}$ W/cm^2, where the physical size of the constrictor was .1 m long by .025 m high. The solution with an initial stagnation pressure of 1 atm diverges, while the solutions with pressures of 6 and 12 atms converge perfectly. The same holds true for a lower limit of velocity where a velocity of 400 m/sec diverges and 600 m/sec gives a converged solution.
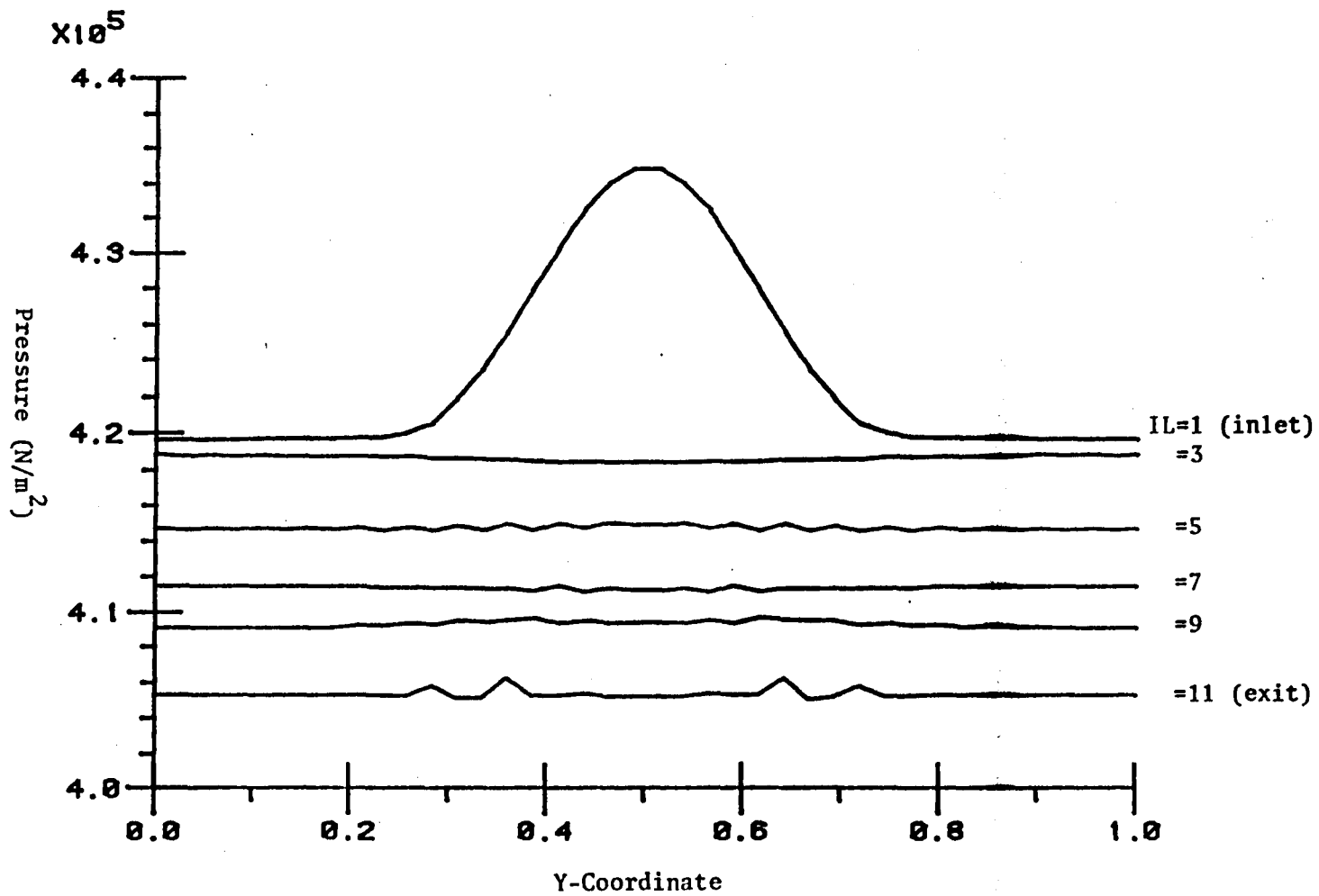
Figure 13. Cross Sectional Pressure Profiles at Various Axial Locations

Chapter IV

CONCLUSIONS AND RECOMMENDATIONS

This paper has described how the two dimensional compressible Navier-Stoke's equations can be solved using an Euler Implicit finite difference solution, with heat addition and boundary conditions representing the constrictor section of an arcjet. The code produces converged solutions for varying boundary and initial conditions, and can show how changing one or more of these conditions can effect the solution.

The temperature profiles prove that the arc energy source does indeed heat up the hydrogen gas passing through the arc. The maximum temperature rise occurs along the centerline where the concentration of energy is the greatest. The overall temperature profile throughout the constrictor closely resembles the gaussian shape of the arc heat intensity. As the heat input is increased, the maximum change in temperature from the initial conditions also increases. The velocity of the gas flow along the centerline decreases at the inlet as a result of interaction with the arc but rises steadily until the exit where the profile suddenly becomes highly inflected. However, outside of the arc

column region, the velocity profile remains uniform and increases linearly. The corresponding pressure effects are opposite except the profile maintains relative uniformity radially while decreasing in the axial direction.

Although the code produces theoretically very accurate results because few simplifying assumptions are made in the solution to the original equations, the range of initial conditions that give converged solutions is prohibitive for extensive research in the area of constricted arcs with large power sources. The fact that the program cannot give a converged solution for power inputs greater than 1×10^{-12} W/cm^2 is a major limitation to the code but it is likely that further research can solve this inadequacy and also provide a code that can produce reliable results in the incompressible velocity range. The Euler Implicit approach to numerically solving the arcjet problem is valid, however more work is needed to extend the range of conditions that will produce converged solutions.

REFERENCES

1. Electric Thruster Performing for Orbit Raising and
    Maneuvering, H. R. Kaufman and R. S. Robinson. AIAA-
    82-1247, 1982. 18th Joint Propulsion Conference.

2. Physics of Electric Propulsion, R. Jahn, McGraw Hill,
    1968.

3. Development of a Regeneratively Cooled 300kW Arcjet
    Engine, James P. Todd and Ronald E. Sheets, AIDD
    Journal, Vol. 3, No. 1, January 1965, pp. 122-126.

4. The Theoretical Enthalpy Distribution of Air in Steady
    Flow Along the Axis of a Direct-Current Electric Arc,
    H. Stine and V. Watson. NASA TN D-1331, August 1962.

5. Arc-Jet Thrustor for Space Propulsion, L. Wallner, J.
    Czika, NASA TN D-2868, 1965.

6. Comparison of Detailed Numerical Solutions with
    Simplified Theories for the Characteristics of the
    Constricted-Arc Plasma Generator, V. Watson, Proceed-
    ings of the 1965 Heat Transfer and Fluid Mechanics
    Institute.

7. Arcjet Engine Performance: Experiment and Theory, R.
    John, S. Bennett, J. Connors. Avco Corporation, AIAA
    Journal, Vol. 1, No. 11, November 1963.

8. Numerical Calculations for the Characteristics of a Gas
    Flowing Axially Through a Constricted Arc, V. Watson,
    E. Pegot. NASA TN D-4042, June 1967.

9. Arc Jet Design, P. Masser, Electric Propulsion Develop-
    ment, Vol. 9, 1962, pp. 69-77.

10. Axisymmetric Flow in Electric Arc Jets and Nozzles, P.
    Masser, AIAA 20th Joint Propulsion Conference, June
    1984, AIAA-84-1385.

11. A two Dimensional Analysis of Laser Heat Addition in
    Converging Nozzles, G. Molvik, D. Choi, C. Merkle.
    AIAA 22nd Aerospace Sciences Meeting, January 1984,
    AIAA-84-0529.

12. Numerical Techniques for Laser Heat Addition, G.
    Molvik, Master's Thesis, Penn. State University, 1984.

13. Computation of Incompressible Flow by a Coupled
    Implicit Scheme, Douchul Choi, Ph.D. Thesis, Penn.
    State University, August 1985.

14. A General Formulation of Alternating Direction Methods,
    Part I, Parabolic and Hyperbolic Problems, Douglas, J.,
    and Gunn, J. E., Numerische Mathematik, Vol. 6, 1964,
    p. 428.

15. Pivoting and Block Tridiagonal Systems, D. Prather,
    ARL, Penn. State University, Notes for AE/ME 526.

APPENDIX

Expanded Form of the Governing Equations

Beginning with the two dimensional vector form of the governing equations

$$\frac{\partial Q}{\partial t} + \frac{\partial E}{\partial x} + \frac{\partial F}{\partial y} = \frac{\partial V}{\partial x} + \frac{\partial W}{\partial y} + H$$

Expanding each of the vectors Q, E, F, V, and W gives the four equations of continuity, x-momentum, y-momentum and energy.

1) $\quad \frac{\partial \rho}{\partial t} + \frac{\partial (\rho u)}{\partial x} + \frac{\partial (\rho v)}{\partial y} = 0$

2) $\quad \frac{\partial (\rho u)}{\partial t} + \frac{\partial (\rho u^2 + p)}{\partial x} + \frac{\partial (\rho u v)}{\partial y} = \lambda(\frac{\partial u}{\partial x} + \frac{\partial v}{\partial y}) + \mu(\frac{\partial u}{\partial x} + \frac{\partial v}{\partial y}) + 2\mu\frac{\partial u}{\partial x}$

3) $\quad \frac{\partial (\rho v)}{\partial t} + \frac{\partial (\rho u v)}{\partial x} + \frac{\partial (v^2 + p)}{\partial y} = \lambda(\frac{\partial u}{\partial x} + \frac{\partial v}{\partial y}) + \mu(\frac{\partial u}{\partial x} + \frac{\partial v}{\partial y}) + 2\mu\frac{\partial v}{\partial y}$

4) $\quad \frac{\partial (\rho e)}{\partial t} + \frac{\partial (e+p)u}{\partial x} + \frac{\partial (e+p)v}{\partial y} = 2\mu(\frac{\partial u}{\partial y} + \frac{\partial v}{\partial x}) + \lambda(\frac{\partial u}{\partial x} + \frac{\partial v}{\partial y})u$

$\qquad + \lambda(\frac{\partial u}{\partial x} + \frac{\partial v}{\partial y})v + 2\mu(\frac{\partial u}{\partial x}u + \frac{\partial v}{\partial y}v) + K\frac{\partial T}{\partial x} + \frac{\partial T}{\partial y})$

where K = thermal conductivity, μ = viscosity, and

λ = second coefficient of viscosity which are tabulated values.

42

End of Document